JASA Express Letters

Design of resonant elastodynamic metasurfaces to control S0 Lamb waves using topology optimization

--Manuscript Draft--

Manuscript Number:	JASA-EL-02141R1
Full Title:	Design of resonant elastodynamic metasurfaces to control S0 Lamb waves using topology optimization
Article Type:	Regular Article
Corresponding Author:	Parisa Shokouhi Pennsylvania State University UNITED STATES
First Author:	Daniel Giraldo Guzman
Order of Authors:	Daniel Giraldo Guzman
	Lalith Sai Srinivas Pillarisetti
	Sashank Sridhar
	Clifford Lissenden
	Mary Frecker
	Parisa Shokouhi
Section/Category:	Structural Acoustics and Vibration
Keywords:	Topology optimization; locally resonant metasurface; Lamb wave propagation
Abstract:	Control of guided waves has applications across length scales ranging from surface acoustic wave devices to seismic barriers. Resonant elastodynamic metasurfaces present attractive means of guided wave control by generating frequency stop-bandgaps using local resonators. This work addresses the systematic design of these resonators using a density-based topology optimization formulated as an eigenfrequency matching problem that tailors antiresonance eigenfrequencies. The effectiveness of our systematic design methodology is presented in a case study, where topologically optimized resonators are shown to prevent the propagation of S0 wave mode in an aluminum plate.
Additional Information:	
Question	Response
Please read the Instructions for full information. Select the appropriate information below to verify that you have consented to this copyright licensing and the conditions and representations set forth in the Instructions.	CC-BY - Creative Commons Attribution 4.0 International License

Design of resonant elastodynamic metasurfaces to control S_0 Lamb waves using topology optimization

Daniel Giraldo Guzman,[1] Lalith Sai Srinivas Pillarisetti,[2] Sashank Sridhar,[2] Cliff J. Lissenden,[2] Mary Frecker,[1] and Parisa Shokouhi[2, a)]

[1)] *Department of Mechanical Engineering, The Pennsylvania State University, University Park, PA 16801, USA*

[2)] *Department of Engineering Science and Mechanics, The Pennsylvania State University, University Park, PA 16801, USA*

dzg5526@psu.edu,
ljp5518@psu.edu,
sps6177@psu.edu,
cjl9@psu.edu,
mxf36@psu.edu,
pxs990@psu.edu

(Dated: 20 October 2022)

Abstract: Control of guided waves has applications across length scales ranging from surface acoustic wave devices to seismic barriers. Resonant elastodynamic metasurfaces present attractive means of guided wave control by generating frequency stop-bandgaps using local resonators. This work addresses the systematic design of these resonators using a density-based topology optimization formulated as an eigenfrequency matching problem that tailors antiresonance eigenfrequencies. The effectiveness of our systematic design methodology is presented in a case study, where topologically optimized resonators are shown to prevent the propagation of S0 wave mode in an aluminum plate.

[a] Author to whom correspondence should be addressed.

1. Introduction

The concept of metamaterials for electromagnetic wave propagation control was introduced by Pendry et al. (Pendry *et al.*, 2006) and Leonhardt (Leonhardt, 2006) for synthetic photonic crystals rarely used before the 2000s (Colquitt *et al.*, 2017). Following this photonic crystals concept, phononic crystals rely on Bragg scattering to create negative elastic modulus and effective mass density, resulting in bandgaps for electromagnetic or elastic waves (Deymier, 2013). However, their reliance on Bragg scattering often results in large-scale structures for low-frequency applications, which might not be practical to realize. To alleviate this limitation, a family of metamaterials called locally resonant metamaterials has been introduced with properties deriving from the local resonances of their sub-wavelength sized constituent unit cells (Fang *et al.*, 2006; Lemoult *et al.*, 2013; Liu *et al.*, 2000). Since their inception, resonant elastodynamic metamaterials have been widely used to control elastic guided waves in plates (Hakoda *et al.*, 2019; Rupin *et al.*, 2014; Xiao *et al.*, 2012), pipes (Danawe *et al.*, 2020; Okudan *et al.*, 2021) and half-space (Colombi *et al.*, 2016b; Garova *et al.*, 1999; Khelif *et al.*, 2010) for applications spanning different length scales. Locally resonant metamaterials intended to control elastic guided waves with local resonators attached to the waveguide surface are sometimes referred to as locally resonant elastodynamic metasurfaces (Colquitt *et al.*, 2017).

Extensive work has been done in designing electromagnetic or acoustic metamaterials in recent years (Ahmed *et al.*, 2021; Amirkulova *et al.*, 2022; Jiang and Fan, 2020), such as designing acoustic metamaterials using deep learning, reinforce learning, or generative adversarial networks (Gurbuz *et al.*, 2021; Lai *et al.*, 2021; Shah *et al.*, 2021). However, the state-of-the-art design of locally resonant elastodynamic metasurfaces still relies on arrays of simple resonator geometries, *e.g.*, rods (Rupin *et al.*, 2014), holes (Brûlé *et al.*, 2014), cuboids, beams, trusses (Zaccherini *et al.*, 2020), four-arm resonators (Hakoda *et al.*, 2019) or mass-spring systems (Palermo and Marzani, 2018). These metasurface designs are accomplished through parametric tuning of dispersion curves empirically until the desired bandgap is achieved; a rational design process is lacking. The objective of this research is to address this gap by proposing a systematic design methodology for locally resonant metasurfaces, *i.e.*, to design resonating structures that can be coupled to a waveguide surface, ultimately controlling the propagation of elastic waves. In search of methodologies that fulfill a set of design requirements, including manipulation of resonances or antiresonances matching them to desired frequencies, structural optimization methods arise as prime candidates (Campbell *et al.*, 2019).

Structural optimization has become an indispensable tool in simulation-based designs through size, shape, material, and topology optimization (Andersen *et al.*, 2019; Guo and Cheng, 2010; Mei and Wang, 2021). The applications are diverse, including vibration control of structures by passive, active, semi-active, or hybrid schemes (El-Khoury and Adeli, 2013; Huang *et al.*, 2011; Kim *et al.*, 2012; Sun *et al.*, 2009). Among the commonly used design techniques, the Topology Optimization Method (TOM) (Bens0e and Kikuchi, 1988; Sigmund and Bendsøe, 2004) provides a systematic design approach. Initially intended to solve structural design problems, the TOM is nowadays used in solving diverse multi-physics problems in mechanics, acoustics, fluids, optics, electromagnetics, materials, among others (Gao *et al.*, 2020; Jihong *et al.*, 2021; Sigmund and Maute, 2013).

The design of acoustic metamaterials using the TOM has been growing in recent years (Dong *et al.*, 2021; Lu *et al.*, 2013; Noguchi *et al.*, 2018). However, the TOM has been only used in a few works to design of elastodynamic metamaterials to manipulate wave propagation. Oh *et al.* (2015) improved an empirically-designed hyperbolic metamaterial using the TOM. Dong *et al.* (2017) used an evolutionary algorithm-based TOM to design metamaterials that exhibit cloaking effects for longitudinal or transverse waves. Yang and Kim (2018) presented a metamaterial exhibiting perfect mode conversion from longitudinal to transverse waves or vice versa using a homogenization TOM. Ahn *et al.* (2019) developed a metamaterial to reflect longitudinal waves at any desired angle using a density-based TOM. Similarly, Rong and Ye (2020) used a genetic algorithm-based TOM to create metamaterials that steer bulk plane waves by tailoring phase delays. To the best of our knowledge, the TOM has not been used to design locally resonant elastodynamic metasurfaces by topologically optimizing three-dimensional resonators through tailoring their antiresonances.

2. Topology optimization

A fundamental mechanism to manipulate the propagation of elastic waves is to purposefully change the displacement boundary conditions on the waveguide surface. This can be achieved by attaching resonant structures to the waveguide surface with antiresonances in the frequency range of interest (*i.e.*, the desired bandgap) (Lissenden *et al.*, 2021). An antiresonance occurs when a system's response to a harmonic force at a given point is zero. Resonators' having antiresonances at a particular frequency results in the reported waveguide clamping effect at that frequency (Antonakakis *et al.*, 2014; Galvagni and Cawley, 2011; Hakoda *et al.*, 2019). We exploit this phenomenon for resonator design by formulating a topology optimization problem such that a resonator's antiresonances are matched with a set of target frequencies. The antiresonance frequencies are obtained by solving a modified-eigenvalue problem (Jeong *et al.*, 2003), *i.e.*, computing eigenfrequencies while constraining the degrees of freedom where the harmonic force would be applied. The resulting frequency solutions are hereafter referred to as *antiresonance eigenfrequencies*.

In order to design resonators, we use a density-based topology optimization formulated as a generalized problem that systematically modifies a resonator's antiresonance eigenfrequencies (f_q) until the target (g_q) is achieved. To that end, the objective function quantifies the relative error between the resonator's antiresonances eigenfrequencies and a reference set of target frequencies, with an L2-norm summing the cumulative error over all the eigenfrequencies, while a set of scalar weights controls each mode influence. The topology optimization process starts with a limited amount of material distributed in a fixed design domain discretized with a fixed number of finite elements N_e. A pseudo-density value ρ_e is assigned to each finite element to describe solid, void, or soft/intermediate elements. Thus, the design variables are the element pseudo-densities. The optimization problem is therefore formulated as shown in Eq. (1);

$$
\begin{aligned}
\min_{\rho} \quad & f(\rho) = \left[\sum_{q=1}^{m} w_q \left(\frac{f_q - g_q}{g_q} \right)^2 \right]^{1/2} \\
\text{s.t.} \quad & V_{min} \leq \sum_{e=1}^{N_e} \rho_e V_e \leq V_{max} \\
& 0 < \rho_{min} \leq \rho_e \leq 1 \\
& \left([K] - \lambda_q [M] \right) \{\Phi_q\} = 0
\end{aligned}
\tag{1}
$$

where m is the total number of eigenmodes considered, w_q is the q^{th} weighting coefficient, N_e is the number of finite elements, $\rho_e V_e$ is the effective volume of each element, V_{max} and V_{min} are respectively the maximum and minimum volume constraints, ρ_{min} is the minimum allowed pseudo-density to prevent numerical problems, $[K]$ and $[M]$ are respectively the global stiffness and mass matrices, and $\{\Phi_q\}$ is the q^{th} eigenvector (mode shape) that corresponds to the q^{th} eigenvalue λ_q.

The optimization problem is solved with a Sequential Linear Programming (SLP) method. This gradient-based method requires a linealized objective function. The linealization process, referred to as sensitivity analysis, is carried out with a first-order Taylor series expansion disregarding the constant terms, such that the objective function ($f(\rho)$) can be rewritten as:

$$
\min_{\rho} \quad \nabla f(\rho_0)^T \rho \tag{2}
$$

where ρ_0 is the linearization point. The objective function is then simplified to:

$$\min_{\rho} \left[\sum_{q=1}^{m} w_q \left(\frac{f_q - g_q}{g_q} \right)^2 \right]^{-1/2} \left[\sum_{q=1}^{m} \frac{w_q (f_q - g_q)}{4\pi g_q^2 \sqrt{\lambda_q}} \frac{\partial \lambda_q}{\partial \rho_k} \right] \rho_k \quad (3)$$

where:

$$\frac{\partial \lambda_q}{\partial \rho_k} = \frac{\Phi_q^T \left(\frac{\partial [K]}{\partial \rho_k} - \lambda_q \frac{\partial [M]}{\partial \rho_k} \right) \Phi_q}{\Phi_q^T [M] \Phi_q} \quad (4)$$

The stiffness $[K]$ and mass $[M]$ matrices depend on the material interpolation model and filters chosen. The interpolation model and the filters are needed to promote the generation of solid and void elements, creating well defined topologies. In this work, we use the Rational Approximation of Material Properties (RAMP) model (Stolpe and Svanberg, 2001) as the interpolation model, and a combination of a density filter with a double Heaviside filter (Xu *et al.*, 2010). Thus, the matrices can be written as:

$$[K] = \sum_{e=1}^{N_e} \frac{\rho_e}{1 + p_1(1 - \rho_e)} [k_e] \qquad [M] = \sum_{e=1}^{N_e} \frac{\rho_e}{1 + p_2(1 - \rho_e)} [m_e] \quad (5)$$

where p_1 and p_2 are the penalization factors for stiffness and mass matrices, respectively. Therefore, the matrix derivatives with respect to the pseudo-densities in Eq. 4 simplify to:

$$\frac{\partial [K]}{\partial \rho_i} = \frac{1 + p_1}{[1 + p_1(1 - \rho_i)]^2} [k_i] \qquad \frac{\partial [M]}{\partial \rho_i} = \frac{1 + p_2}{[1 + p_2(1 - \rho_i)]^2} [m_i] \quad (6)$$

3. Results

As our case study, we use the topology optimization problem formulated in Eq. (1) to design resonators (based on antiresonance eigenfrequency matching) to prevent the propagation of the 50 kHz symmetric S_0 mode of Lamb waves in a thin plate; thus setting $m = 1$, $g_1 = 50$

kHz as the target frequency, and f_1 as the antiresonance eigenfrequency to be optimized. By generating an antiresonance at the contact interface between the resonator's base (surface in the xy plane at $z = 0$) and the waveguide surface, a displacement boundary condition ($u_x = 0$ and $u_y = 0$) is applied to the waveguide surface when an S_0 wave impinges upon the resonator, therefore clamping the surface displacement and preventing the transmission of S_0 waves. Provided that a continuity condition at the contact interface between the resonator's base and the waveguide surface is satisfied, it is possible to design a single resonator without including the waveguide or neighboring resonators. To do so, the waveguide is replaced with a harmonic load at the resonator's base equivalent to the load the wave mode would exert. Thus, the design problem is reduced to optimizing a single resonator. Attaching multiple optimized resonators to the waveguide surface constitutes a locally resonant metasurface.

Depending on the initial parameters chosen, the optimization problem may yield different solutions. Here, we present two selected solutions to demonstrate the design of resonators using the TOM. A list of common initial parameters used to obtain both solutions are shown in Table 1. The main difference between the two solutions is the minimum volume allowed in each case. For the first solution, the minimum volume is $V_{min} = 3\%$ while V_{min} is increased to 10% to obtain the second solution. Although this may seem like a subtle difference, it allows the optimization to distribute the material differently, therefore resulting in different topologies. Hereinafter, we call the first solution the Elephant-like topology, and the second solution the Boat-like topology, as shown in Fig. 1. We note that a symmetry condition along the wave propagation direction is imposed to reduce computational cost.

Table 1. Optimization initial parameters

Material properties	Young's modulus $E = 70 \times 10^9$ Pa, Mass density $m = 2700$ kg/m^3
Design domain	Dimensions: $25 \times 12.5 \times 25$ mm, Discretization: $16 \times 8 \times 16$ elements
Material Model and filters	RAMP model with $p = 3$. Density filter plus Heaviside filter
Volume constraints	Maximum volume $V_{max} = 20\%$, Minimum volume variable.

The left hand side of images in Fig. 1 are a half-symmetric representation of the pseudo-densities (ρ_e) distributed in the design domain, *i.e.*, a fixed volume with a fixed finite element mesh discretization. Each finite element has an associated pseudo-density value that ranges from 0 to 1, with 0 representing a void element, and 1 a fully solid element. The void elements are depicted as white voxels, and the solid elements as black voxels. Those with intermediate pseudo-density values are illustrated with varying shades of gray. The right hand side of images in Fig. 1 show the final post-processed topologies after recovering the symmetry condition. Note that during the post processing, the pseudo-density values are converted into a well-defined shape using the TOPslicer program developed by Zegard and Paulino (Zegard and Paulino, 2016), then the topology is re-meshed and analyzed with a commercial finite elements software.

As a consequence of post-processing, the dynamic response of the optimized topologies differs from the original optimized solution. Fig. 2(a) presents the normalized Frequency Response Functions (FRFs) for the post-processed topologies in Fig. 1 at the center point of each topology's base. These plots are obtained by applying a harmonic load at the base of each resonator in the x-direction (in-plane) since the S_0 Lamb wavestructure is predominantly in-plane displacement (see Fig. 2(b),(c)). The FRFs in Fig. 2(a) show an antiresonance at 51.6 kHz for the Elephant-like topology, marked as a vertical solid red line. This frequency is slightly deviated from the target of 50 kHz due to the post-processing smoothing process. For the Boat-like topology, although an antiresonance appears at 50.1 kHz (vertical solid line), the corresponding dip is not as "deep" as the one observed for the Elephant-like topology. Since a displacement boundary condition is expected to be better imposed if the antiresonance is more pronounced (i.e., the dip in the FRF is deeper and has a smaller amplitude), we expect to observe a better performance in preventing wave propagation for the Elephant-like topology. Also note the distance between the antiresonance and its closest resonance peaks, marked a vertical dashed red lines. For the Elephant-like topology, the two closest resonances peaks, at 44.4 kHz and 66.7 kHz, are more separated than they are for the Boat-like topology with the closest peaks at 39.1 kHz and 50.9 kHz. This observation suggests the Elephant-like resonators could generate a wider transmission bandgap (Colombi *et al.*, 2016a,b).

To evaluate both topologies' responses, frequency-domain simulations are performed using the model shown in Fig. 3(a) consisting of a plate with an arrangement of either topologically optimized resonator. Both the plate and the resonators are modeled as aluminum with material properties from Table 1. The topology-optimized resonators' effectiveness in suppressing an incident S_0 Lamb wave mode is validated at their identified antiresonance

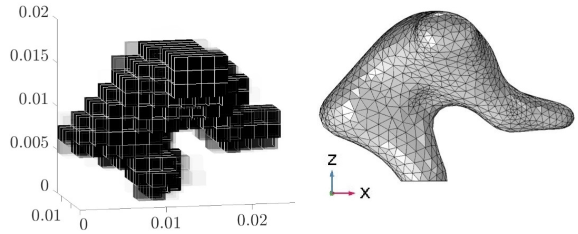

(a) Elephant-like topology.

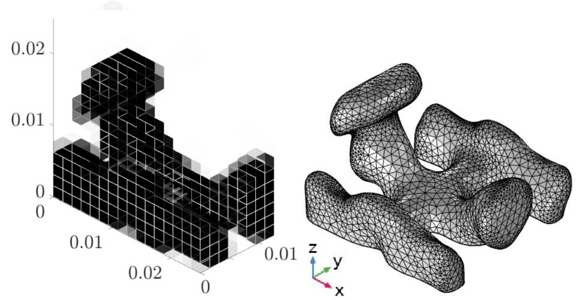

(b) Boat-like topology.

Fig. 1. Two exemplary topology-optimized resonators. Raw topologies (left images), and post-processed topologies (right images).

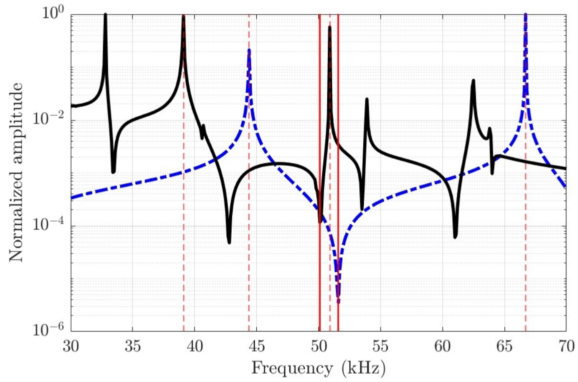

(a) FRFs of topology-optimized resonators

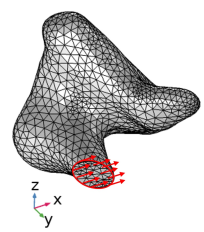

(b) Harmonic force on Elephant-like.

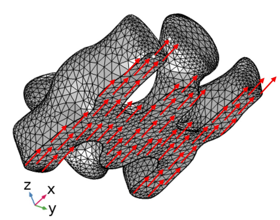

(c) Harmonic force on Boat-like.

Fig. 2. Harmonic response for optimized resonators. (a) Blue dashed line is FRF of Elephant-like resonator, black solid line is FRF of Boat-like resonator, vertical red solid lines are antiresonances, vertical red dashed lines are resonances. (b) and (c) Harmonic forces applied on optimized topologies' base represented as red arrows.

frequencies (see Fig. 2) by performing frequency-domain finite element analyses using the structural mechanics module in COMSOL Multiphysics. The plate has been divided into three analysis regions: *incident*, *metasurface*, and *transmission* region. The buffer regions prevent numerical errors by allowing the propagating wave to transition to the absorbing layers which prevent wave reflections from the model boundaries. The plate supports a staggered arrangement of three rows of resonators with five or four units per row. An S_0 Lamb wave generated in the body-load excitation region propagates towards the metasurface region through the incident region. By the time the spherical wave impinges on the arrangement of resonators, the wavefront is close to planar.

Fig. 3 shows the harmonic response of the Elephant-like and Boat-like topologies at 51.6 kHz and at 50 kHz, corresponding to their respective antiresonance frequencies. Note that the absorbing layer and the buffer regions shown in Fig. 3(a) are not shown in the other sub-figures. Fig. 3(b) presents the baseline simulation, i.e., S_0 Lamb wave propagation in the plate without resonators. Fig. 3(c),(d) show that in presence of resonator arrays, a portion of the energy is reflected and the remaining propagates through the transmission region. To quantify the reflected and transmitted proportions, normalized wavenumber spectra for the incident and transmission regions are computed by a spatial Fourier transformation of the complex total displacements extracted at the center of incident and transmission regions, respectively. The incident, reflected, and transmitted wave modes are identified from the wavenumber spectra as shown in Fig. 4. The peaks with positive wavenumbers indicate wave modes propagating backward, whereas the peaks with negative wavenumbers denote waves propagating forward.

The body-load excites a pure S_0 Lamb wave mode propagating in the positive x-direction, resulting in the largest peak in the wavenumber spectra of Fig. 4. We observe reflection and mode-conversion of the incident wave energy as an S_0 mode and as a mode-

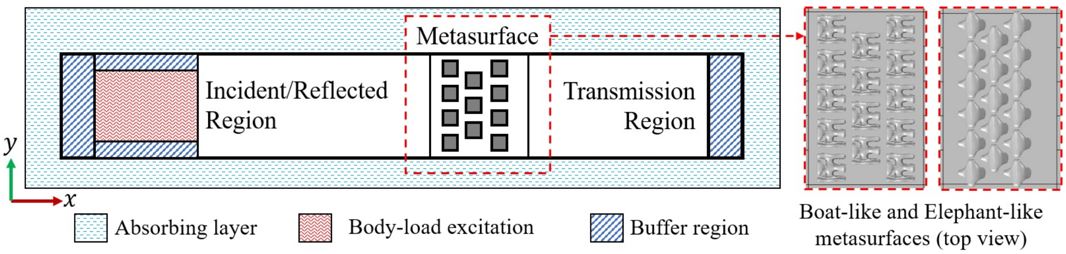

(a) Schematic representation of a plate composed of three regions: incident, metasurface, transmission. Optimized resonators are arranged in the metasurface region.

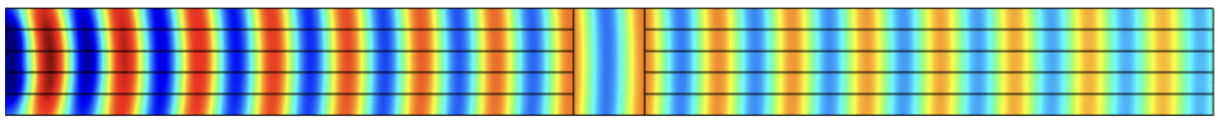

(b) Baseline simulation for S_0 Lamb wave propagation.

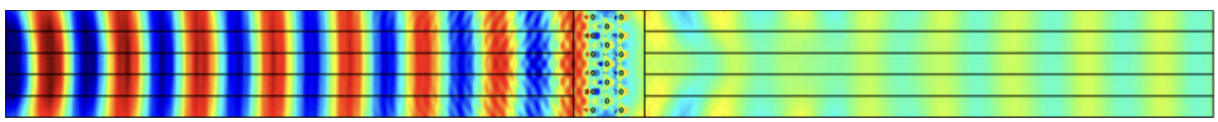

(c) Metasurface composed of 17 Elephant-like resonators.

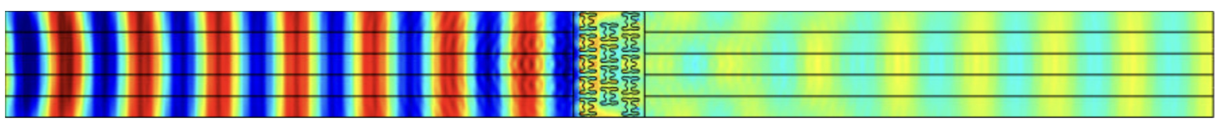

(d) Metasurface composed of 14 Boat-like resonators.

Fig. 3. Numerical analysis of optimized metasurfaces. (a) Schematic model for simulation, (b) baseline simulation, (c) and (d) Harmonic in-plane displacement field for locally resonant metasurfaces composed of topology-optimized resonators.

converted A_0 mode for both the resonator configurations. For the case of the Elephant-like topology, most of the incident wave energy is reflected as low-amplitude S_0 and A_0 modes observed as backward propagating waves in the incident region. Quantitatively, 25.2% of the S_0 mode is transmitted, and the remaining is converted into an A_0 mode with 4.8% normalized amplitude, as shown in the transmission region of Fig. 4(a). On the other hand, the Boat-like topology allows 47.2% of S_0 mode transmission, as well as a 31% transmission

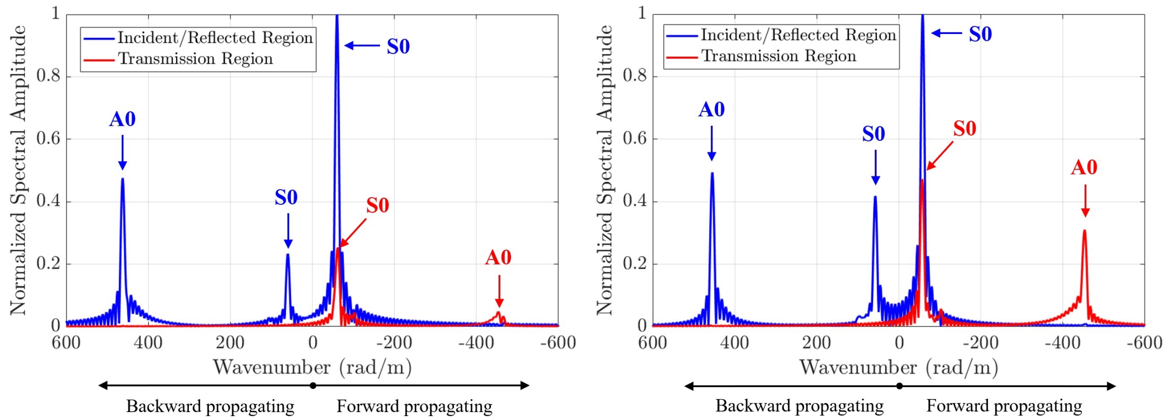

(a) Elephant-like wavenumber spectrum. (b) Boat-like wavenumber spectrum.

Fig. 4. Wavenumber spectra for metasurfaces of Figure 3.

as a mode-converted A_0 mode, making it the less effective topology in preventing wave propagation. Similarly, some of the wave energy is reflected as S_0 and A_0 modes, observed as backward propagating waves in Fig. 4(b).

These results demonstrate that both optimized resonators are suppressing the S_0 Lamb wave mode by imposing the desired antiresonance on the plate. The higher suppression of the incident S_0 mode for the Elephant-like topology compared to the Boat-like topology is an evidence for its higher efficiency. However, since the mode-conversions between the S_0 and A_0 modes are non-intuitive, the resonators' bases cover different surface areas in the metasurface region (Fig. 3(c)(d)), and the antiresonances occur at different frequencies, therefore a direct comparison of their performances is not straightforward. Based on these observations, both optimized resonators suppress the propagation of S_0 Lamb wave mode albeit with different efficiency, providing fundamental understanding about the mechanisms involved in the control of elastic wave propagation while showing the feasibility of local resonator design using structural optimization techniques.

4. Conclusions

In this paper, we present a design methodology formulated as a topology optimization problem to design resonators using a density-based and gradient-based topology optimization method. This methodology can be used to systematically design locally resonant elastodynamic metasurfaces comprising the topology-optimized resonators mounted on a waveguide. Our approach requires a resonator's antiresonance eigenfrequency to match a predefined target frequency, generating a bandgap around that frequency. We demonstrate the potential of this methodology for designing resonant metasurfaces that suppress S_0 Lamb waves. Nonetheless, this method can be extended to the design of resonant metasurfaces to control other types of elastic waves such as surface waves regardless of the frequency range, making this approach suitable for designing resonant structures at multiple length scales. Moreover, this design methodology can be generalized to tailor not only antiresonances but resonances or even both simultaneously, presenting a potential approach to widen metasurface's frequency bandgaps and to design acoustic metamaterials.

Acknowledgments

The authors gratefully acknowledge the support of the National Science Foundation under Grant No. 1934527. Any opinions, findings, and conclusions or recommendations expressed in this material are those of the author(s) and do not necessarily reflect the views of the National Science Foundation.

Computations for this research were performed on the Pennsylvania State University's Institute for Computational and Data Sciences' Roar supercomputer.

References and links

Ahmed, W. W., Farhat, M., Zhang, X., and Wu, Y. (**2021**). "Deterministic and probabilistic deep learning models for inverse design of broadband acoustic cloak," Physical Review Research **3**(1), 013142.

Ahn, B., Lee, H., Lee, J. S., and Kim, Y. Y. (**2019**). "Topology optimization of metasurfaces for anomalous reflection of longitudinal elastic waves," Computer Methods in Applied Mechanics and Engineering **357**, 112582.

Amirkulova, F. A., Gerges, S., and Norris, A. N. (**2022**). "Broadband acoustic lens design by reciprocity and optimization," JASA Express Letters **2**(2), 024005.

Andersen, P. R., Henriquez, V. C., Sanchis, L., and Sánchez-Dehesa, J. (**2019**). *Design of multi-directional acoustic cloaks using two-dimensional shape optimization and the boundary element method* (Universitätsbibliothek der RWTH Aachen).

Antonakakis, T., Craster, R., and Guenneau, S. (**2014**). "Moulding and shielding flexural waves in elastic plates," EPL (Europhysics Letters) **105**(5), 54004.

Bens0e, M., and Kikuchi, N. (**1988**). "Generating optimal topologies in structural design using a homogenization method, comp," Meths. Appl. Mechs. Engng **71**, 197–224.

Brûlé, S., Javelaud, E., Enoch, S., and Guenneau, S. (**2014**). "Experiments on seismic metamaterials: molding surface waves," Physical review letters **112**(13), 133901.

Campbell, S. D., Sell, D., Jenkins, R. P., Whiting, E. B., Fan, J. A., and Werner, D. H. (**2019**). "Review of numerical optimization techniques for meta-device design," Optical Materials Express **9**(4), 1842–1863.

Colombi, A., Colquitt, D., Roux, P., Guenneau, S., and Craster, R. V. (**2016**a). "A seismic metamaterial: The resonant metawedge," Scientific reports **6**(1), 1–6.

Colombi, A., Roux, P., Guenneau, S., Gueguen, P., and Craster, R. V. (**2016**b). "Forests as a natural seismic metamaterial: Rayleigh wave bandgaps induced by local resonances," Scientific reports **6**(1), 1–7.

Colquitt, D., Colombi, A., Craster, R., Roux, P., and Guenneau, S. (**2017**). "Seismic metasurfaces: Sub-wavelength resonators and rayleigh wave interaction," Journal of the Mechanics and Physics of Solids **99**, 379–393.

Danawe, H., Okudan, G., Ozevin, D., and Tol, S. (**2020**). "Conformal gradient-index phononic crystal lens for ultrasonic wave focusing in pipe-like structures," Applied Physics Letters **117**(2), 021906.

Deymier, P. A. (**2013**). *Acoustic metamaterials and phononic crystals*, **173** (Springer Science & Business Media).

Dong, H.-W., Zhao, S.-D., Miao, X.-B., Shen, C., Zhang, X., Zhao, Z., Zhang, C., Wang, Y.-S., and Cheng, L. (**2021**). "Customized broadband pentamode metamaterials by topology optimization," Journal of the Mechanics and Physics of Solids **152**, 104407.

Dong, H.-W., Zhao, S.-D., Wang, Y.-S., and Zhang, C. (**2017**). "Topology optimization of anisotropic broadband double-negative elastic metamaterials," Journal of the Mechanics and Physics of Solids **105**, 54–80.

El-Khoury, O., and Adeli, H. (**2013**). "Recent advances on vibration control of structures under dynamic loading," Archives of Computational Methods in Engineering **20**(4), 353–360.

Fang, N., Xi, D., Xu, J., Ambati, M., Srituravanich, W., Sun, C., and Zhang, X. (**2006**). "Ultrasonic metamaterials with negative modulus," Nature materials **5**(6), 452–456.

Galvagni, A., and Cawley, P. (**2011**). "The reflection of guided waves from simple supports in pipes," The Journal of the Acoustical Society of America **129**(4), 1869–1880.

Gao, J., Xiao, M., Zhang, Y., and Gao, L. (**2020**). "A comprehensive review of isogeometric topology optimization: methods, applications and prospects," Chinese Journal of Mechanical Engineering **33**(1), 1–14.

Garova, E., Maradudin, A., and Mayer, A. (**1999**). "Interaction of rayleigh waves with randomly distributed oscillators on the surface," Physical Review B **59**(20), 13291.

Guo, X., and Cheng, G.-D. (**2010**). "Recent development in structural design and optimization," Acta Mechanica Sinica **26**(6), 807–823.

Gurbuz, C., Kronowetter, F., Dietz, C., Eser, M., Schmid, J., and Marburg, S. (**2021**). "Generative adversarial networks for the design of acoustic metamaterials," The Journal of the Acoustical Society of America **149**(2), 1162–1174.

Hakoda, C., Lissenden, C. J., and Shokouhi, P. (**2019**). "Clamping resonators for low-frequency s0 lamb wave reflection," Applied Sciences **9**(2), 257.

Huang, M., Tse, K., Chan, C. M., and Lou, W. (**2011**). "Integrated structural optimization and vibration control for improving wind-induced dynamic performance of tall buildings," International Journal of Structural Stability and Dynamics **11**(06), 1139–1161.

Jeong, W. B., Yoo, W. S., and Kim, J. Y. (**2003**). "Sensitivity analysis of anti-resonance frequency for vibration test control of a fixture," KSME international journal **17**(11), 1732–1738.

Jiang, J., and Fan, J. A. (**2020**). "Simulator-based training of generative neural networks for the inverse design of metasurfaces," Nanophotonics **9**(5), 1059–1069.

Jihong, Z., Han, Z., Chuang, W., Lu, Z., Shangqin, Y., and Zhang, W. (**2021**). "A review of topology optimization for additive manufacturing: Status and challenges," Chinese Journal of Aeronautics **34**(1), 91–110.

Khelif, A., Achaoui, Y., Benchabane, S., Laude, V., and Aoubiza, B. (**2010**). "Locally resonant surface acoustic wave band gaps in a two-dimensional phononic crystal of pillars on a surface," Physical Review B **81**(21), 214303.

Kim, W., Song, Y. H., and Kim, J. E. (**2012**). "Topology optimization of actuator arms in hard disk drives for reducing bending resonance-induced off-tracks," Structural and Multidisciplinary Optimization **46**(6), 907–912.

Lai, P., Amirkulova, F., and Gerstoft, P. (**2021**). "Conditional wasserstein generative adversarial networks applied to acoustic metamaterial design," The Journal of the Acoustical Society of America **150**(6), 4362–4374.

Lemoult, F., Kaina, N., Fink, M., and Lerosey, G. (**2013**). "Wave propagation control at the deep subwavelength scale in metamaterials," Nature Physics **9**(1), 55–60.

Leonhardt, U. (**2006**). "Optical conformal mapping," Science **312**(5781), 1777–1780.

Lissenden, C. J., Hakoda, C. N., and Shokouhi, P. (**2021**). "Control of low-frequency lamb wave propagation in plates by boundary condition manipulation," Journal of Applied Physics **129**(9), 094903.

Liu, Z., Zhang, X., Mao, Y., Zhu, Y., Yang, Z., Chan, C. T., and Sheng, P. (**2000**). "Locally resonant sonic materials," science **289**(5485), 1734–1736.

Lu, L., Yamamoto, T., Otomori, M., Yamada, T., Izui, K., and Nishiwaki, S. (**2013**). "Topology optimization of an acoustic metamaterial with negative bulk modulus using local resonance," Finite Elements in Analysis and Design **72**, 1–12.

Mei, L., and Wang, Q. (**2021**). "Structural optimization in civil engineering: A literature review," Buildings **11**(2), 66.

Noguchi, Y., Yamada, T., Izui, K., and Nishiwaki, S. (**2018**). "Optimum design of an acoustic metamaterial with negative bulk modulus in an acoustic-elastic coupled system using a level set–based topology optimization method," International Journal for Numerical Methods in Engineering **113**(8), 1300–1339.

Oh, J. H., Ahn, Y. K., and Kim, Y. Y. (**2015**). "Maximization of operating frequency ranges of hyperbolic elastic metamaterials by topology optimization," Structural and Multidisciplinary Optimization **52**(6), 1023–1040.

Okudan, G., Danawe, H., Ozevin, D., and Tol, S. (**2021**). "Torsional wave focusing in cylindrical structures with the conformal gradient-index phononic crystal lens," Journal of Applied Physics **129**(17), 174902.

Palermo, A., and Marzani, A. (**2018**). "Control of love waves by resonant metasurfaces," Scientific Reports **8**(1), 1–8.

Pendry, J. B., Schurig, D., and Smith, D. R. (**2006**). "Controlling electromagnetic fields," Science **312**(5781), 1780–1782.

Rong, J., and Ye, W. (**2020**). "Multifunctional elastic metasurface design with topology optimization," Acta Materialia **185**, 382–399.

Rupin, M., Lemoult, F., Lerosey, G., and Roux, P. (**2014**). "Experimental demonstration of ordered and disordered multiresonant metamaterials for lamb waves," Physical Review Letters **112**(23), 234301.

Shah, T., Zhuo, L., Lai, P., De La Rosa-Moreno, A., Amirkulova, F., and Gerstoft, P. (**2021**). "Reinforcement learning applied to metamaterial design," The Journal of the Acoustical Society of America **150**(1), 321–338.

Sigmund, O., and Bendsøe, M. P. (**2004**). "Topology optimization–from airplanes to nanooptics," in *BRIDGING from technology to society: DTU 1829-2004-175 år* (Technical University of Denmark), pp. 40–51.

Sigmund, O., and Maute, K. (**2013**). "Topology optimization approaches," Structural and Multidisciplinary Optimization **48**(6), 1031–1055.

Stolpe, M., and Svanberg, K. (**2001**). "An alternative interpolation scheme for minimum compliance topology optimization," Structural and Multidisciplinary Optimization **22**(2), 116–124.

Sun, H., Yang, Z., Li, K., Li, B., Xie, J., Wu, D., and Zhang, L. (**2009**). “Vibration suppression of a hard disk driver actuator arm using piezoelectric shunt damping with a topology-optimized pzt transducer,” Smart Materials and Structures **18**(6), 065010.

Xiao, Y., Wen, J., and Wen, X. (**2012**). “Flexural wave band gaps in locally resonant thin plates with periodically attached spring–mass resonators,” Journal of Physics D: Applied Physics **45**(19), 195401.

Xu, S., Cai, Y., and Cheng, G. (**2010**). “Volume preserving nonlinear density filter based on heaviside functions,” Structural and Multidisciplinary Optimization **41**(4), 495–505.

Yang, X., and Kim, Y. Y. (**2018**). “Topology optimization for the design of perfect mode-converting anisotropic elastic metamaterials,” Composite Structures **201**, 161–177.

Zaccherini, R., Colombi, A., Palermo, A., Dertimanis, V. K., Marzani, A., Thomsen, H. R., Stojadinovic, B., and Chatzi, E. N. (**2020**). “Locally resonant metasurfaces for shear waves in granular media,” Physical Review Applied **13**(3), 034055.

Zegard, T., and Paulino, G. H. (**2016**). “Bridging topology optimization and additive manufacturing,” Structural and Multidisciplinary Optimization **53**(1), 175–192.